JFM RAPIDS
journals.cambridge.org/rapids

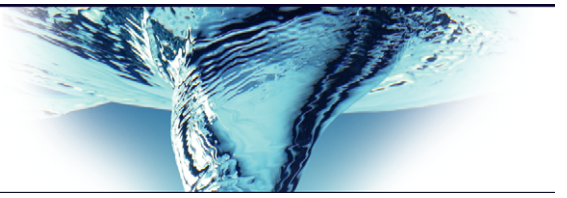

Lift generation with optimal elastic pitching for a flapping plate

Diing-wen Peng† and Michele Milano

Department of Mechanical and Aerospace Engineering, University at Buffalo, 318 Jarvis Hall, Buffalo, NY 14260-4400, USA

(Received 26 September 2012; revised 16 November 2012; accepted 10 December 2012; first published online 7 February 2013)

The lift-generating capabilities of a translating and passively pitching rectangular plate are assessed experimentally. The plate pitch dynamics are generated by a rotational spring, and a genetic algorithm isolates a set of spring parameters maximizing the average lift. Our experiments identified a range of parameters that produce kinematic trajectories associated with optimal lift production. The stroke length and the dynamic response of the spring at the driving frequency are revealed to play crucial roles in the generation of such trajectories. Measurements taken with digital particle image velocimetry are used to analyse the results.

Key words: biological fluid dynamics, flow–structure interactions, swimming/flying

1. Introduction

Flapping wings have long intrigued biologists and engineers alike, particularly in the context of insect flight. Ellington (1984) showed that leading-edge vortices (LEV) generated by insect wings play a key role in lift production; this pioneering work has been followed by studies for two-dimensional (Ellington 1996; Dickinson & Götz 1993) and three-dimensional (Liu, Ellington & Kawachi 1998; Birch & Dickinson 2001) cases. Dickinson (1999) studied the lift generated by a flapping fruitfly wing experimentally, and Ramamurti & Sandberg (2002) performed the same studies using simulations. In these studies, wings were considered to be rigid bodies.

More recent efforts have focused on the interaction between elastic flapping wings and the associated flow. Among the computational studies on the subject, Bergou, Xu & Wang (2007) showed that the aerodynamic and inertial forces equally contribute to the passive pitching of a plate with torsional elasticity concentrated at the leading edge. Eldredge, Toomey & Medina (2010) investigated a two-link structure where the rotational kinematics of the upper link are prescribed, while the second link is attached with a torsional spring and allowed to pitch passively. A similar structure

† Email address for correspondence: dpeng2@buffalo.edu

doi:10.1017/jfm.2012.614

was also investigated by Vanella *et al.* (2009). In these studies, lift generation is fairly consistent over a range of phase differences between pitching and heaving. Vanella *et al.* (2009) also examined the flow structure to establish the effect of natural frequency on the formation of leading-edge vortices and wake capture mechanisms.

Ishihara, Horie & Denda (2009*a*) explored a lumped torsional flexibility model, concluding that lift generation from purely passive pitching is a possibility. Ishihara *et al.* (2009*b*) and Tanaka, Whitney & Wood (2011) explored the same setup experimentally, reaching similar conclusions. Zhang, Liu & Lu (2010) used a similar model in the context of fish-like propulsion, and showed that the ratio between the natural frequency of the spring and the heaving frequency affects the direction of propulsion. They also identified a region of non-periodic motion based on the frequency ratio. Dai, Luo & Doyle (2012) simulated a plate with distributed elasticity in three-dimensions, and examined the relative importance of wing inertia and aerodynamic load on the deformation. An important relationship resulting from these studies is the effect of frequency ratio on the phase shift between the plate's heaving and passively pitching motion. Dickinson (1999) examined the effects of this phase shift on aerodynamic forces and flow structures. Ramananarivo, Godoy-Diana & Thiria (2011) assumed inertia to be the dominating force in passive pitching, and showed that the interplay between heaving–pitching phase difference and aerodynamics has a key role in propulsive efficiency. Kim & Gharib (2011) linked the increase in the forces acting on a flexible plate to the delayed development of three-dimensional vortex formation. Khan, Steelman & Agrawal (2009) approached the passive pitching mechanism from a design perspective, by optimizing a set of nonlinear spring parameters to maximize the lift based on a quasi-unsteady model.

This paper aims to characterize the relationships between natural frequency and damping ratio of an elastically mounted flapping plate that produces positive average lift, i.e. optimal in the context of hovering motion. We set up an experiment using a flat plate free to translate in a direction perpendicular to its long axis, following a purely sinusoidal motion, while another motor rotates the plate about its long axis. A model-following controller is designed such that the behaviour of a spring can be precisely emulated by the rotational motor. The amplitude and frequency of the sinusoidal translation of the plate are fixed, and the spring parameters are optimized to maximize the average lift force produced during three translation periods of the plate, starting from a still-water condition. The optimization is performed by the same clustering genetic algorithm used by Milano & Gharib (2005) to uncover families of lift-maximizing kinematics for a flapping plate.

Here the genetic algorithm produces families of spring parameters that maximize the average lift measured in a stationary reference frame. Using full force and torque measurements, as well as digital particle image velocimetry (DPIV) measurements of the corresponding vortical structures, we present a full comparison between optimal and suboptimal lift-generating dynamics. Separate optimization experiments are performed for different translation amplitudes. These experiments show that the optimal average lift decreases significantly beyond a limiting range of amplitudes, and highlight important factors that determine optimal lift generation. The phase and magnitude responses of the springs at the translation frequency are also identified as crucial parameters in understanding the resulting trajectories associated with the optimal parameters.

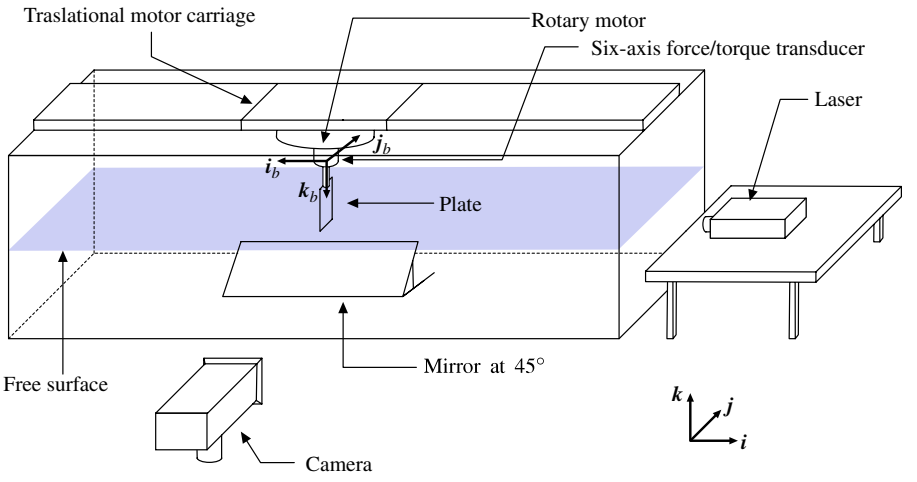

FIGURE 1. Experimental setup shown with arbitrarily placed but properly oriented lab frame $\{\boldsymbol{i},\boldsymbol{j},\boldsymbol{k}\}$. The body frame $\{\boldsymbol{i}_b,\boldsymbol{j}_b,\boldsymbol{k}_b\}$ is attached to the transducer, which rigidly connects to the plate in series. The DPIV camera is positioned to capture the motion in a plane parallel to $\{\boldsymbol{i},\boldsymbol{j}\}$ through the inclined mirror.

2. Problem definition and experimental setup

The goal of the experiment is to maximize the average lift generated by a rectangular plate with two degrees of freedom, i.e. rotation and translation. The experimental setup is shown in figure 1. The acrylic plate used is 5.1 mm thick with chord length $c = 40$ mm and aspect ratio of 6. The plate is attached to a six-axis force transducer and a rotational motor, and the assembly is driven by a translation motor at the base plate. The translational trajectory is a simple sinusoid of the form:

$$x(t) = \tfrac{1}{2}[A\cos(\Omega t) + A], \tag{2.1}$$

where A is defined as the stroke length associated with each half-stroke. The direction $x(t)$ is along the translational motor rail and parallel to the unit vector $\boldsymbol{i}$ shown in figure 1. The location $x = A/2$ is defined to be the centre of the tank, and the distance from the plate to the walls at any instant is at least $10c$ to minimize the interference from reflected waves. A Reynolds number of 10^4 (based on the plate chord length and maximum translational velocity U_{max}) is chosen with room-temperature water as the medium, consistent with the upper range for insect flight (Wang 2005). The translational period and angular frequency are defined as $T = \pi A/U_{max}$ and $\Omega = 2\pi/T$ respectively. The numerical values of these parameters are listed in table 1. We performed separate optimization experiments for different stroke lengths between the range of $A = 2.5c$ and $A = 10c$ to examine the effect of travel distance on the optimal lift attainable with passive pitching.

A model-following controller allows accurate emulation of a wide range of elastic parameters for the rotational mount. The emulated model for the elastically mounted plate is:

$$\ddot{\theta} + 2\zeta\omega_n\dot{\theta} + \omega_n^2\theta = \frac{1}{J}M_f, \tag{2.2}$$

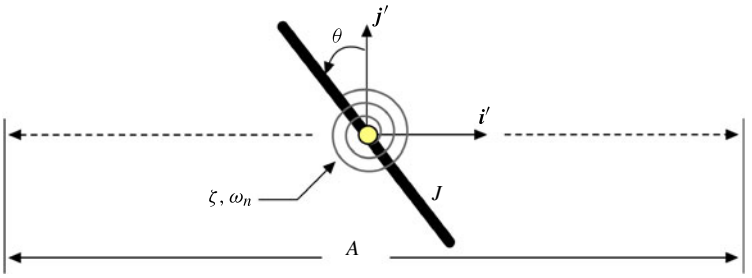

FIGURE 2. The elastic plate is modelled as a second-order system with natural frequency ω_n, damping ratio ζ and moment of inertia J about the pivot at the half-chord location. The angle convention is as shown for the convenience of emulation. The frame $\{\boldsymbol{i}',\boldsymbol{j}'\}$ maintains the same orientation as the lab frame $\{\boldsymbol{i},\boldsymbol{j}\}$ shown in figure 1 but travels with the plate through the stroke length A.

A (m):	$2.50c$	$3.00c$	$4.00c$	$5.00c$	$6.00c$	$7.00c$	$10.0c$
T (s):	1.25	1.50	2.00	2.50	3.00	3.50	5.01
Ω (rad s^{-1}):	5.02	4.18	3.14	2.51	2.09	1.79	1.255

TABLE 1. Representative optimization experiment configurations. The Reynolds number is 10 000 for all cases, based on chord length $c = 40.0$ mm and peak velocity $U_{max} = 0.251$ m s^{-1}.

where ζ and ω_n are the damping ratio and natural frequency of the emulated spring, respectively. θ is the plate angle as illustrated in figure 2, and $J = 0.0005$ kg m^2 is the moment of inertia of the plate. The torque acting on the plate M_f is measured, and an internal Runge–Kutta integrator propagates the states to prescribe the upcoming point in the trajectory, providing in real time the correct reference signal to the rotational motor. Zero initial conditions $\theta(0) = \dot{\theta}(0) = 0$ are used. The control loop runs at 100 Hz, whereas the highest translation frequency used in our experiments is 0.89 Hz.

The optimization problem is posed as:

$$\max_{\zeta,\omega_n} \overline{L} = \frac{1}{R}\sum_{i=1}^{R}\left|\frac{1}{3T}\int_{3T}^{6T} L_i(t)\,\mathrm{d}t\right|, \tag{2.3}$$

where $R = 7$ is the number of trials repeated for each set of ζ and ω_n to account for measurement errors. L_i is the time-varying lift generated from trial i, defined as the force along the $\boldsymbol{j}$-direction. The average is taken of the last three periods out of a total of six periods for each trial, thus excluding the initial transient dynamics from the optimization. The absolute value accounts for the fact that plate motion can start with either positive or negative θ depending on the initial moment imbalance on the plate. The resulting kinematic trajectory of each run is saved by the emulator, allowing precise playback of the same trajectory for digital particle image velocimetry measurements.

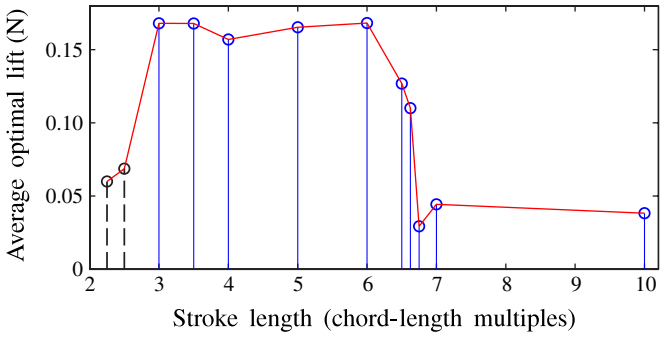

FIGURE 3. Average cost of optimal population versus stroke length. Pitching responses associated with $A = 2.25c$ and $2.5c$ fail to settle into steady state within 6 periods; their average costs are shown here as dashed stems.

3. Results from the genetic algorithm

A genetic algorithm is used to tune the model parameters of the spring emulator such that average lift is maximized. The algorithm was developed in Milano & Koumoutsakos (2002) in the context of drag reduction over a cylinder in cross-flow, and used by Milano & Gharib (2005) in producing optimal kinematic parameters associated with the maximum lift of a flapping plate. The algorithm started with an initial population of $n = 50$, where a population member is a particular combination of ζ and ω_n. The algorithm systematically searches the parameter space and evolves the population to approximate the set of parameters that yield maximum lift. Convergence is declared when the average lift values corresponding to 90 % of parameters in the population are within the sensitivity of the force transducer, ± 0.0285 N.

Average costs associated with the converged populations are shown in figure 3 for different stroke lengths. The pitching motions associated with $A = 2.25c$ and $A = 2.5c$ are unable to reach steady state within 6 periods as specified by (2.3); thus our discussion is focused on $A \geqslant 3c$. Two distinct regions emerge from the result: stroke lengths between $3c$ and $6c$ produce optimal average lifts that are an order of magnitude higher than for the longer stroke lengths. The optimal parameter clusters for various stroke lengths are shown in figure 4; these clusters approximate the set of parameters that produces lift-maximizing oscillations. The trends exhibit by different stroke lengths can be clarified by considering phase and magnitude responses associated with the spring, which is discussed in § 6.

We pick two representative stroke lengths, $A = 5c$ and $A = 10c$, from the high-lift and low-lift region respectively, for comparison. The global cluster of ζ and ω_n for the $A = 5c$ case can be interpreted by considering the relative stiffness and damping of the systems: low values of natural frequency signify 'soft' springs, for which small disturbances in the forcing cause larger pitch angles; conversely, high values of natural frequency are associated with stiff springs, in which case the plate remains at $\theta = 0$ throughout the run. The two clusters shown for $A = 10c$ can be explained in a similar fashion. However, the longer stroke length and period significantly limit the lift generation. Our subsequent analyses are first restricted to these two stroke lengths, in order to gain insight into the effects of stroke length on the lift. Then we explore the effects of flow structures on the lift optimality, by considering a suboptimal case from

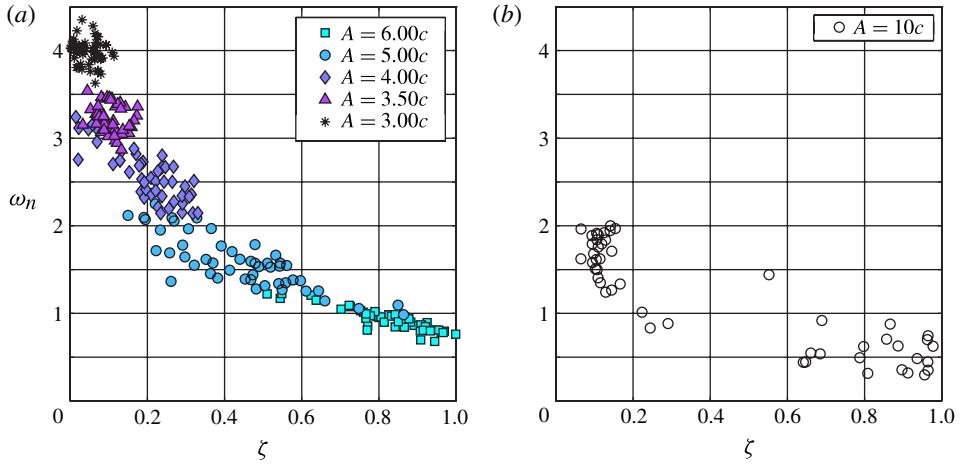

FIGURE 4. Optimal population clusters for stroke lengths with high lift ($A = 3c$–$6c$) (a), compared with a representative low-lift case ($A = 10c$) (b). The optimization bounds are $0.1 \leqslant \zeta \leqslant 1$ and $0.1 \leqslant \omega_n \leqslant 6$ rad s^{-1}. Only the region containing converged points is shown.

Case	A (m)	ζ	ω_n (rad s^{-1})	L_{avg} (N)	$\overline{L}$ (N)	Description
1	$5c$	0.35	1.6	0.20	0.22	Optimal (short stroke)
2	$5c$	0.40	1.0	0.18	0.090	Suboptimal (short stroke)
3	$10c$	0.065	1.6	0.047	0.048	Low-ζ optimal (long stroke)
4	$10c$	0.94	0.48	0.039	0.037	High-ζ optimal (long stroke)

TABLE 2. Parameter values for selected cases. We choose a trial k with average lift $L_{avg} = |(1/3T)\int_{3T}^{6T} L_k(t)\,\mathrm{d}t|$ from each case, and use its kinematics for PIV measurements.

outside the optimal cluster for $A = 5c$. The parameter values for these cases are listed in table 2.

4. Stroke length and lift generation

As shown before, the stroke length has a significant effect on the lift; here we compare DPIV measurements for the $A = 5c$ and $A = 10c$ cases at 50 % span. Vorticity fields are plotted along the trajectories for cases $A = 5c$ and $A = 10c$ in figures 5 and 6 respectively, and the lift associated with each frame is labelled in the adjacent plots. For the $A = 10c$ case, we choose to focus on the low-ζ optimal point, since the pitch angle was insignificant for points in the high-ζ cluster. The highest average lift that can be generated for a stroke amplitude $A = 10c$ is one order of magnitude less than for the shorter stroke amplitude. This result suggests that stroke amplitude is crucial for maximum lift generation.

Frames (a) and (b) of figure 5 show the plate at the beginning of the fourth period. The counter-clockwise (CCW) vortex shown near the top-left of the plate in (a) is a previously shed leading-edge vortex (LEV), from the end of the third period (not shown); it drifts downward in (b), revealing a wake capture mechanism

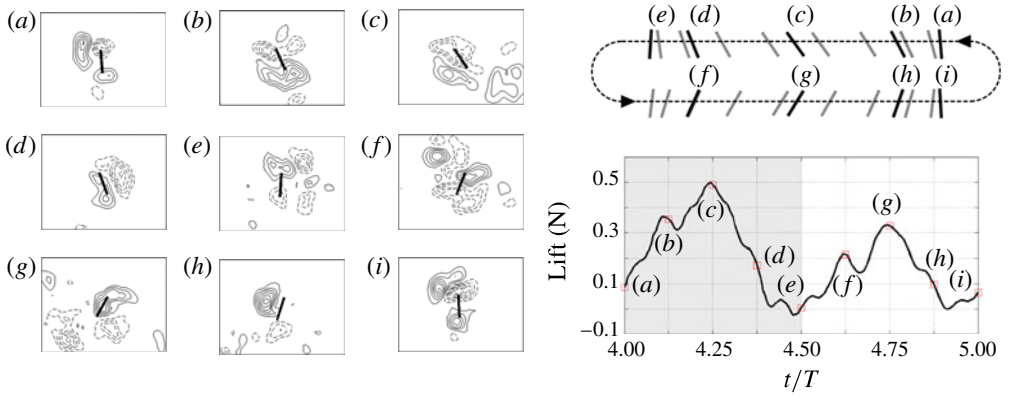

FIGURE 5. Vorticity plots for optimal trajectory ($A = 5c$) over one representative period. The solid contours represent counter-clockwise rotations and dashed lines clockwise rotations. (*a*) $t/T = 4$; (*b*) 4.125; (*c*) 4.25; (*d*) 4.375; (*e*) 4.5; (*f*) 4.625; (*g*) 4.75; (*h*) 4.875; (*i*) 5. The average lift over this particular period is 0.195 N. The kinematic trajectories are shown as temporally equidistant snapshots on the top-right figure, with downstroke on the top row and upstroke on the bottom. The grey and white background colour on the lift plot denotes downstroke and upstroke respectively.

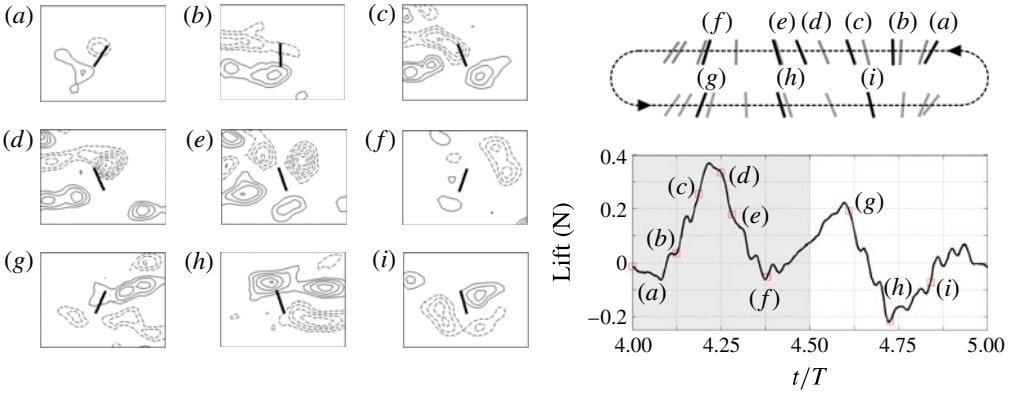

FIGURE 6. As figure 5, but showing plots for optimal trajectory ($A = 10c$) over one representative period. The average lift for this particular period is 0.043 N. (*a*) $t/T = 4$; (*b*) 4.125; (*c*) 4.1875; (*d*) 4.25; (*e*) 4.28; (*f*) 4.38; (*g*) 4.61; (*h*) 4.725; (*i*) 4.84.

(Dickinson 1999), that can also be seen as a minor peak in the lift plot. Frame (*b*) also shows the development of the LEV to the right of the plate due to the translating motion, while the plate rotation produces another CCW vortex to the left of the plate. The secondary vortex, generated from the rotation shown in (*b*), eventually combines with the LEV to form a larger vortex. This combined LEV remains attached, continuing to form as shown in frame (*c*). Due to the short travel distance, the vortices have yet to be fully shed near the end of downstroke at frame (*e*). Frames (*f*–*i*) mirror frames (*b*–*e*).

In contrast with the $A = 5c$ case, the optimal trajectory for $A = 10c$ in figure 6 shows irregular downstrokes and upstrokes: the plate begins with a negative angle of attack in frame (a) as a result of transient responses from the previous period (not shown), settling into a positive angle of attack between (b) and (c); between the same frames, the clockwise (CW) rotation of the plate generates a CCW vortex near the leading edge. Part of the same vortex combines with the LEV, subsequently breaking off before frame (d) due to the return of the angular position to a negative angle of attack.

As remarked, the optimal trajectory for this case yields an average lift one order of magnitude smaller than the $A = 5c$ case. Since this lift is fairly close to the sensitivity of the force transducer, along with fact that the plate fails to lock into a periodic pattern, we suspect that the extremely low value of average lift is the effect of measurement noise. To test this, we ran the emulator with the same set of parameters in air, which produced similar values for the average lift. This confirmed that the optimal lift generated for the $A = 10c$ case is not significant, thus we will limit our discussion to the $A = 5c$ case in the following section.

5. Flow response

Figure 7 compares lift and vorticity for optimal and suboptimal cases. Sequence (a) in figure 7 shows the vorticity after the plate reaches its maximum velocity during the downstroke, revealing that the LEV for the optimal case remains attached for a longer duration. The next sequence (b) immediately follows the stroke reversal, showing a still well-formed (for the optimal case) vortex from the wake of the downstroke. Sequence (c) shows the creation of CW vortices to the left of the plate due to plate rotation in both cases, though the suboptimal case lags behind the optimal case. The optimal case forms the rotation-induced vortex in the first frame and begins to form the LEV in the second frame, whereas the suboptimal case only starts to form the rotation-induced vortex in the second frame. This means that phase differences in the plate trajectory, determined by the spring parameters, are crucial for optimal lift generation. In the next set of frames (d), the plate goes through the stroke reversal at the end of a downstroke. Here the flow structure in the optimal trajectory exhibits similar mechanisms as before, whereas for the suboptimal trajectory there is a significant lag in vortex formation; it can be seen that this lag causes delayed stroke reversals for the suboptimal case. Delayed stroke reversals have been noted in Dickinson (1999) to have detrimental effects on lift generation.

6. Dynamic response of the plate

The optimal population of ζ and ω_n for $A = 5c$ shown in figure 4 can be expressed in terms of the phase and magnitude response for the rotational second-order system in (2.2). The phase ϕ and magnitude G between the output angle and the input moment at the driving frequency Ω are given by the relationships (Ogata 2002):

$$\phi = -\arctan \frac{2\zeta \dfrac{\Omega}{\omega_n}}{1 - \left(\dfrac{\Omega}{\omega_n}\right)^2}, \tag{6.1}$$

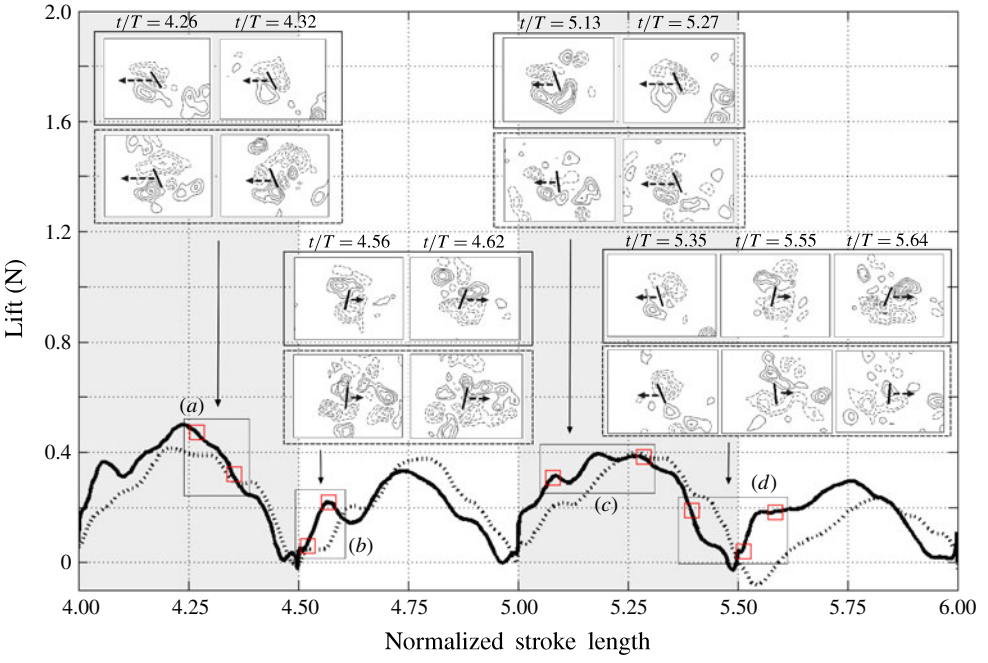

FIGURE 7. Differences in the lift trend between optimal (solid line) and suboptimal (dashed line) trajectories for $A = 5c$. The inset vorticity plots are enclosed in a continuous line frame for the optimal case, and in a broken line frame for the suboptimal case. The arrows represent the current travel direction of the plate and the plate's velocity magnitude (relative to other frames in the plot). The abscissa is normalized by the total travel length of a full stroke ($2A$) to better indicate the particular location of the plates.

$$G = 20\log\left(\frac{1}{J\omega_n^2}\right) - 20\log\sqrt{\left(1-\left(\frac{\Omega}{\omega_n}\right)^2\right)^2 + \left(2\zeta\frac{\Omega}{\omega_n}\right)^2}. \tag{6.2}$$

An analysis of the optimal population (figure 8) shows that both ϕ and G approach Gaussian distributions with means $\overline{\phi} = -138°$ and $\overline{G} = 56.1$ dB, and standard deviations of $S_\phi = 8.09°$ and $S_G = 3.69$ dB. The phase and magnitude of the optimal case we analysed are $-142°$ and 56.8 dB respectively, which is representative of the average values associated with the optimal population. The value of ϕ in this case reveals that the output angle lags behind the input torque by the specified amount as shown in figure 9(*a*), thus providing a link between the translational kinematics, system dynamics, and rotational kinematics.

Given that periodic torque forcing of the plate is possible only if the plate is oriented properly at each quarter-stroke, the plate must reverse its direction with precise timing and allow the pitch angle to build up to the desirable orientation at the quarter-stroke. Additionally, the plate needs to maintain positive, non-vertical angles of attack throughout most of each half-stroke to produce consistently positive lift. Such requirements suggest that pitch reversal must occur near the end of each half-stroke. In essence, the phase shift of the spring response at the driving frequency provides an

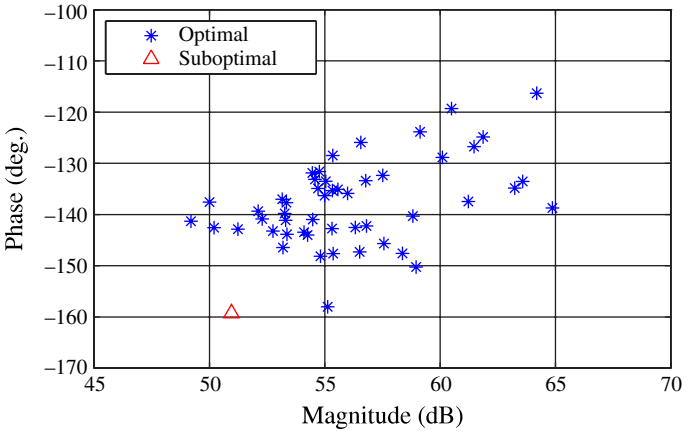

FIGURE 8. Optimal population for $A = 5c$ in terms of magnitude and phase response of the system at the driving frequency $\Omega = 2.51$ rad s^{-1}.

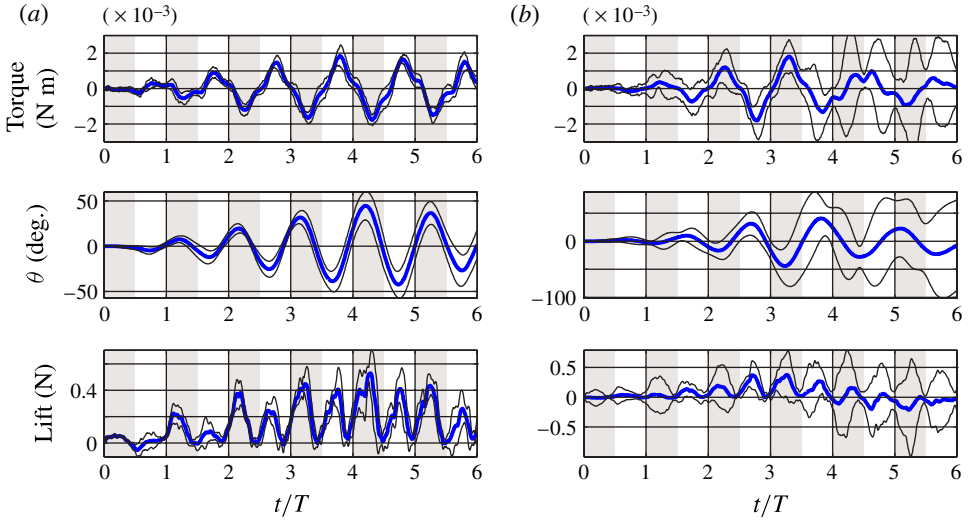

FIGURE 9. The torque, position, and lift of the optimal (*a*) and suboptimal (*b*) cases over seven runs are plotted. The thick line is the mean, and the thin lines are the 2 standard deviation upper and lower bounds. Note that the initial perturbation of angular travel, which determines the subsequent direction of motion, has been unified for all runs. The consistency in behaviour shown by this particular optimal case is also exhibited by all other sets of parameters in the optimal population.

intuitive measure for the timing of pitch reversal. Similarly, the magnitude response is a criterion that must be met to achieve the proper orientation.

The suboptimal case that we analysed has phase of $-159°$ and magnitude of 50.95 dB, placing the point just outside the optimal region as shown in figure 8.

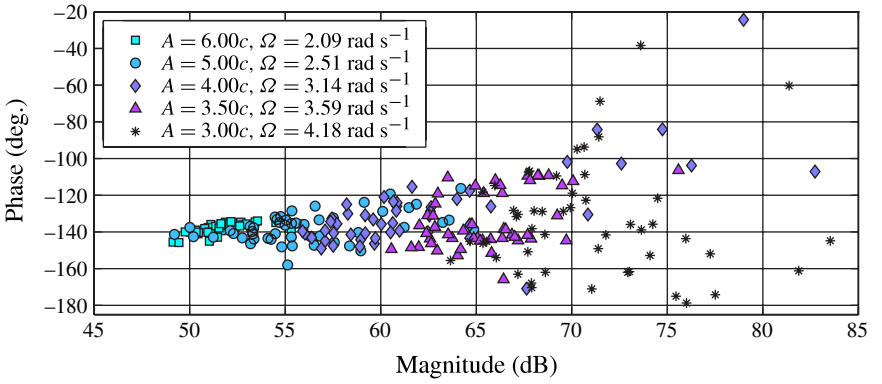

FIGURE 10. Optimal magnitude and phase responses at the driving frequencies associated with different stroke lengths A. The centroids $(\bar{G}, \bar{\phi})_A$ are $(70.3, -134)_{3c}$, $(65.5, -134)_{3.5c}$, $(62.6, -129)_{4c}$, $(56.1, -138)_{5c}$ and $(51.7, -138)_{6c}$.

The phase and magnitude associated with the suboptimal system prevent the plate from locking into a periodic trajectory, which is illustrated in figure 9(*b*) as the torque and angular trajectories for this point become wildly inconsistent across the seven repeated trials.

The phase and magnitude analysis we applied to case $A = 5c$ can be generalized for stroke lengths from $A = 3c$ to $6c$. Figure 10 shows an optimal range of phases (near $-135°$) shared by these high-lift stroke lengths, and reveals that their magnitude decreases with increasing stroke length. The flow structures associated with shorter lengths are characterized by rapid destruction of LEVs before shedding. This premature termination of vortices leads to smaller values of circulation, thus producing less torque on the plate as shown in figure 11. The smaller forcing requires higher amplification for the plate to reach pitch angles similar to longer stroke length cases; hence the inverse relationship between the optimal magnitude and stroke length. Figure 10 also shows that the longer stroke lengths are more sensitive to changes in phase response, since in such cases the timing at which vortices are shed becomes crucial. The shorter stroke lengths are less dependent on the travel length as the vortices are captured by returning strokes before saturation.

Ramananarivo *et al.* (2011) also studied the frequency response of a flexural beam in the context of passive pitching. They assumed inertia to be the primary force contributor, and derived the magnitude and phase relationships between heaving and pitching. In contrast, our phase and magnitude analysis relates the torque to pitching, thus providing an intermediate layer that connects the unsteady flow structures to the plate dynamics and kinematics.

7. Conclusions

We explored the possibility of using elasticity to generate optimal passive pitch reversal for a flapping plate, so as to maximize the lift generated. A key result of this study is that in order for the pitch reversal to occur only near the end of each half-stroke, the translational amplitude needs to be less than approximately 6 times the plate chord length. For larger stroke lengths, our optimizer showed that it is impossible

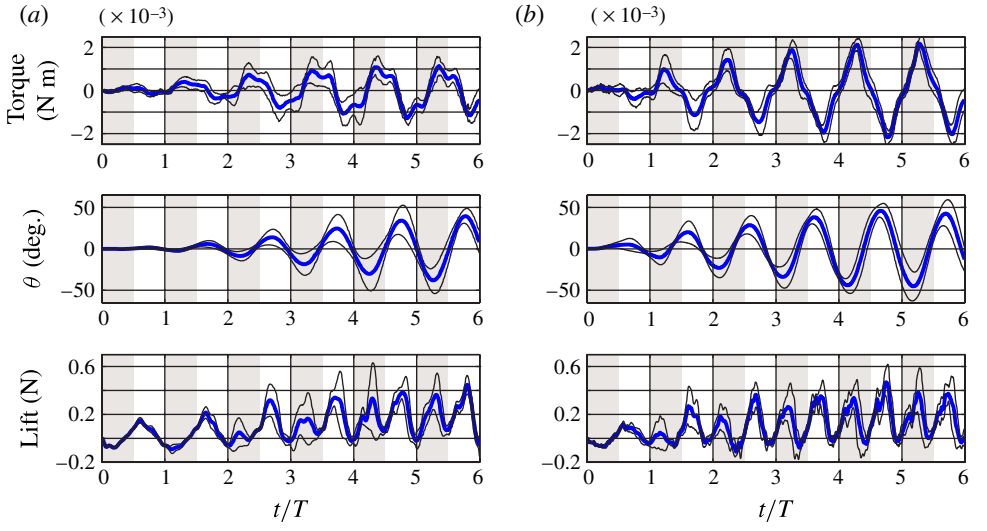

FIGURE 11. The torque, position, and lift of the $A = 3c$ (a) and $A = 6c$ (b) cases over seven trials. Other details are the same as figure 9.

to choose spring parameters that lock the system into a periodic pitching, thereby preventing the flapping plate from generating significant lift.

The other two parameters shown to be critical for optimal lift generation are the magnitude and phase responses of the rotational spring at the plate translation frequency. We identified regions in which these parameters produce maximum average lift, for translation amplitudes between 3 and 6 chord lengths.

References

BERGOU, A. J., XU, S. & WANG, Z. J. 2007 Passive wing pitch reversal in insect flight. *J. Fluid Mech.* **591**, 321–337.

BIRCH, J. M. & DICKINSON, M. H. 2001 Spanwise flow and the attachment of the leading-edge vortex on insect wings. *Nature* **412** (6848), 729–733.

DAI, H., LUO, H. & DOYLE, J. F. 2012 Dynamic pitching of an elastic rectangular wing in hovering motion. *J. Fluid Mech.* **693**, 473–499.

DICKINSON, M. H. 1999 Wing rotation and the aerodynamic basis of insect flight. *Science* **284** (5422), 1954–1960.

DICKINSON, M. H. & GÖTZ, K. G. 1993 Unsteady aerodynamic performance of model wings at low Reynolds numbers. *J. Exp. Biol.* **64**, 45–64.

ELDREDGE, J. D., TOOMEY, J. & MEDINA, A. 2010 On the roles of chord-wise flexibility in a flapping wing with hovering kinematics. *J. Fluid Mech.* **659**, 94–115.

ELLINGTON, C. P. 1984 The aerodynamics of hovering insect flight. V. Vortex theory. *Phil. Trans. R. Soc. Lond.* B **305** (1122), 115–144.

ELLINGTON, C. P. 1996 Leading edge vortices in insect flight. *Nature* **384**, 626–630.

ISHIHARA, D., HORIE, T. & DENDA, M. 2009*a* A two-dimensional computational study on the fluid–structure interaction cause of wing pitch changes in dipteran flapping flight. *J. Exp. Biol.* **212** (Pt 1), 1–10.

ISHIHARA, D., YAMASHITA, Y., HORIE, T., YOSHIDA, S. & NIHO, T. 2009*b* Passive maintenance of high angle of attack and its lift generation during flapping translation in crane fly wing. *J. Exp. Biol.* **212** (Pt 23), 3882–3891.

KHAN, Z., STEELMAN, K. & AGRAWAL, S. 2009 Development of insect thorax based flapping mechanism. *IEEE. Intl Conf. Robot.* 3651–3656.

KIM, D. & GHARIB, M. D. 2011 Flexibility effects on vortex formation of translating plates. *J. Fluid Mech.* **677**, 255–271.

LIU, H., ELLINGTON, C. P. & KAWACHI, K. C 1998 A computational fluid dynamic study of hawkmoth hovering. *J. Exp. Biol.* **201**, 461–477.

MILANO, M. & GHARIB, M. 2005 Uncovering the physics of flapping flat plates with artificial evolution. *J. Fluid Mech.* **534**, 403–409.

MILANO, M. & KOUMOUTSAKOS, P. 2002 A clustering genetic algorithm for cylinder drag optimization. *J. Comput. Phys.* **175** (1), 79–107.

OGATA, K. 2002 *Modern Control Engineering*, 4th edn. Pearson Education.

RAMAMURTI, R. & SANDBERG, W. C. 2002 A three-dimensional computational study of the aerodynamic mechanisms of insect flight. *J. Exp. Biol.* **205** (10), 1507–15018.

RAMANANARIVO, S., GODOY-DIANA, R. & THIRIA, B. 2011 Rather than resonance, flapping wing flyers may play on aerodynamics to improve performance. *Proc. Natl Acad. Sci. USA* **108** (15), 5964–5969.

TANAKA, H., WHITNEY, J. P. & WOOD, R. J. 2011 Effect of flexural and torsional wing flexibility on lift generation in hoverfly flight. *Integr. Comput. Biol.* **51** (1), 142–150.

VANELLA, M., FITZGERALD, T., PREIDIKMAN, S., BALARAS, E. & BALACHANDRAN, B. 2009 Influence of flexibility on the aerodynamic performance of a hovering wing. *J. Exp. Biol.* **212** (1), 95–105.

WANG, Z. J. 2005 Dissecting insect flight. *Annu. Rev. Fluid Mech.* **37**, 183–210.

ZHANG, J., LIU, N.-S. & LU, X.-Y. 2010 Locomotion of a passively flapping flat plate. *J. Fluid Mech.* **659**, 43–68.